Monte Carlo studies of the radiation fields in the Linac Coherent Light Source undulators and of the corresponding signals in the Čerenkov beam loss monitors

Mario SANTANA LEITNER [1*], Alberto FASSÒ [1], Alan S. FISHER [1], Heinz D. NUHN [1], Jeffrey C. DOOLING [2], William BERG [2] and Bin. X. YANG [2]

[1] *SLAC National Accelerator Laboratory, Menlo Park, CA, 94025, USA*
[2] *Argonne National Laboratory, Argonne, IL, 60439, USA*

In 2009 the Linac Coherent Light Source (LCLS) at the SLAC National Accelerator Center started free electron laser (FEL) operation. In order to continue to produce the bright and short-pulsed x-ray laser demanded by FEL scientists, this pioneer hard x-ray FEL requires a perfectly tailored magnetic field at the undulators, so that the photons generated at the electron wiggling path interact at the right phase with the electron beam. In such a precise system, small (>0.01%) radiation-induced alterations of the magnetic field in the permanent magnets could affect FEL performance.

This paper describes the simulation studies of radiation fields in permanent magnets and the expected signal in the detectors. The transport of particles from the radiation sources (i.e. diagnostic insert) to the undulator magnets and to the beam loss monitors (BLM) was simulated with the intra nuclear cascade codes FLUKA and MARS15. In order to accurately reproduce the optics of LCLS, lattice capabilities and magnetic fields were enabled in FLUKA and betatron oscillations were validated against reference data. All electron events entering the BLMs were printed in data files. The paper also introduces the Radioactive Ion Beam Optimizer (RIBO) Monte Carlo 3-D code, which was used to read from the event files, to compute Čerenkov production and then to simulate the optical coupling of the BLM detectors, accounting for the transmission of light through the quartz.

KEYWORDS: undulator, demagnetization, beam loss monitor, BLM, Čerenkov, FLUKA, RIBO, Monte Carlo

I. Introduction

The Linac Coherent Light Source (LCLS) at the SLAC National Accelerator Center in Stanford University has been operating since April 2009. This pioneer free electron laser machine produces hard x-rays a billion times brighter than those in modern synchrotrons sources, with ultra fast pulses that enable scientists to take stop-motion pictures of atoms and molecules in motion. The 33 undulators of LCLS are the key component in the generation of this laser. Each of them contains an array of 225 perfectly tailored magnets that make the electron beam pulses wiggle at the right frequency for the *self-amplified spontaneous emission* (SASE) effect to take place. Vigilance over these complex components is mandatory to maintain their performance[1)]. For example, state-of-the-art sensors and associated systems adjust the position of the undulators, and the temperature of the tunnel and of the supports is controlled. In a longer time scale, the undulators are threatened by the radiation fields in the tunnel, because their alternate magnetic field is generated by radiation-sensitive $Nd_2Fe_{14}B$ permanent magnets. It is estimated that the FEL could be compromised once the undulators were demagnetized by as little as 0.01 %. SLAC and APS have put in place a program to protect LCLS undulators from radiation, which comprises machine protection system (MPS) instrumentation, dosimetry and extensive computer simulations.

1. APS Beam Loss Monitors

As part of LCLS MPS, large solid-angle Čerenkov detector beam loss monitors have been tested and installed at intervals of eight segments, i.e. BLM01 before segment 01, 09, 17, 25 and 33. Lost and deviated electrons as well as their subsequent descendants generated in electromagnetic showers along the undulator create Čerenkov light in their path through the high-purity fused-silica (12.77 cm wide, 6.29 cm high, and 0.64 cm thick), which envelopes the beam pipe as a tunning-fork. The fused-silica radiator is encased in an anodized aluminum coated housing that enables efficient transport of the Čerenkov photons via internal reflection through a tapered region and stem into the photocathode of a compact photomultiplier tube (PMT), which, in turn, provides low electrical noise signals, as it does not detect lower energy x-rays.

Computation of the optical efficiency of the radiator η_c, which accounts for the absorption losses at each reflection and *through* the silica[a] is performed by the Monte Carlo random-walk simulation code RIBO[2)].

*Corresponding Author, E-mail: msantana@slac.stanford.edu

[a] This effect is negligible for optical photons in silica

Work supported in part by US Department of Energy contract DE-AC02-76SF00515.

2. Monte Carlo implementation of the LCLS undulator

FLUKA[3,4] intra nuclear cascade code has been used to model almost the entire LCLS for radiation protection studies[5]. MARS15[6] has also been used for similar purposes in several areas of LCLS, and a dedicated MARS model of the undulator was created at APS to validate and supplement the results provided by FLUKA. Both models include a detailed implementation of the undulator geometry, including all their magnets and poles, interstitial quadrupoles and the beam loss monitors, the tunnel, etc. Since a reduced set of objects is repeated many times, a virtual gallery was created in the FLUKA model for 'cyber-storage' of the prototypes, and 'lattice' mapping instructions were coded to replicate the prototypes along the tunnel. **Figure 1** shows a 3D *Povray*[7] rendering of the geometry of the prototypes and of the resulting beamline, as implemented in FLUKA.

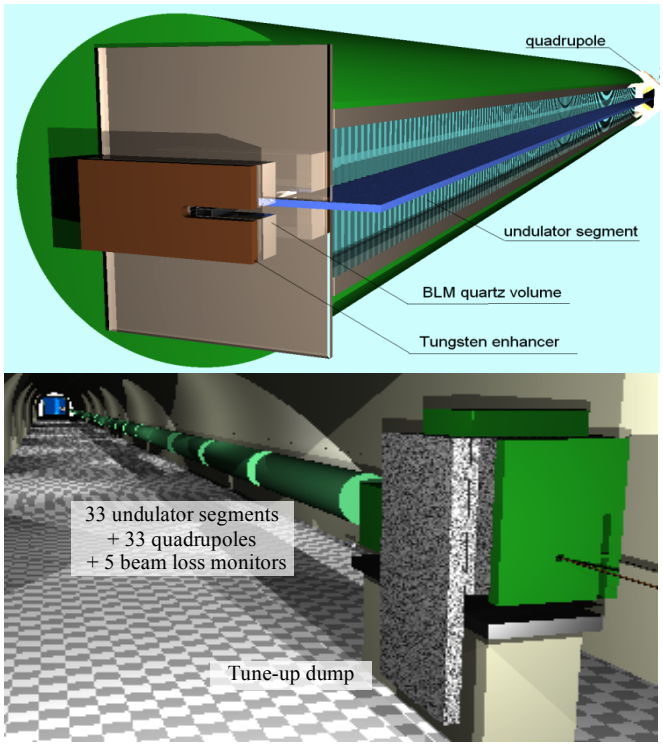

Fig. 1 Povray 3-D rendering of (top) a BLM and undulator unit, and (bottom) the entire LCLS undulator tunnel, as implemented in FLUKA.

Quadrupole focusing in the 132 m undulator section was implemented both in FLUKA and MARS15. Step-sizes were adjusted to maintain optimal tracking with moderate CPU consumption. **Figure 2** shows the accurate reproduction of betatron oscillations with FLUKA or MARS at nominal energy (13.6 GeV). Tests at other energies (4.3 GeV) were equally satisfactory.

In order to improve statistics, several variance reduction techniques were used. For example, in FLUKA leading particle biasing and multiple scattering were activated and the probability of interaction in thin insertion devices was artificially increased (and the reaction products accordingly outweighed). Similarly, photoneutron reactions were enhanced.

.

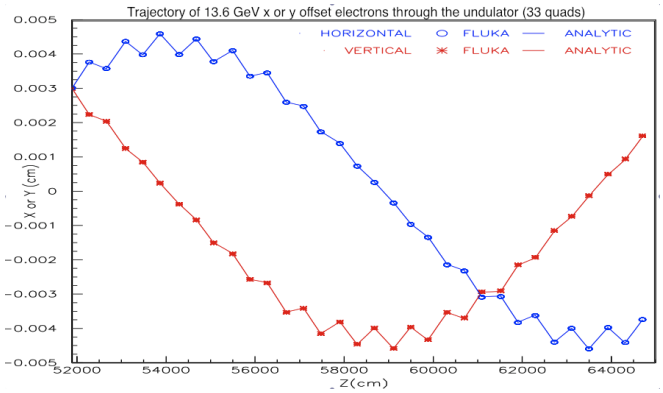

Fig. 2 Comparison of simulated (circles or dots) and analytical (solid line) trajectories along the 33 segments of the undulator for electrons starting with 30 micron offset (horizontal or vertical).

3. Monte Carlo simulation of the Beam Loss Monitors

(1) First analysis of the optical efficiency

Although FLUKA can transport optical photons by defining some advanced-user routines and setting up various parameters, in this case we used a lighter code for the optical transport. RIBO was designed for transport of radioactive ions through vacuum systems, but it can equally be used to simulate photons reflecting within a fiber, etc.

A first order study that was presented in[8] is briefly summarized here.

We implemented the fork geometry of the radiator and analyzed the optical efficiency of the LCLS BLMs as a function of the electron impacting position for normally incident electrons. To do so, in RIBO's user customizable particle source routine we defined the Čerenkov birth direction in the surface of a **z**-cone of semi-angle 47.1° (which corresponds to relativistic electrons in fused silica, equation 1). The birth coordinates were uniformly sampled with the BLM volume. In absence of relevant absorption by the silica, photons were only deviated at the quasi-elastic collisions with the aluminum coating. The RIBO custom printing function was adjusted to write the initial coordinates, number of collisions and flight path of every photon from birth to collection at the PMT. The optical efficiency was obtained as the average transmission intensity.

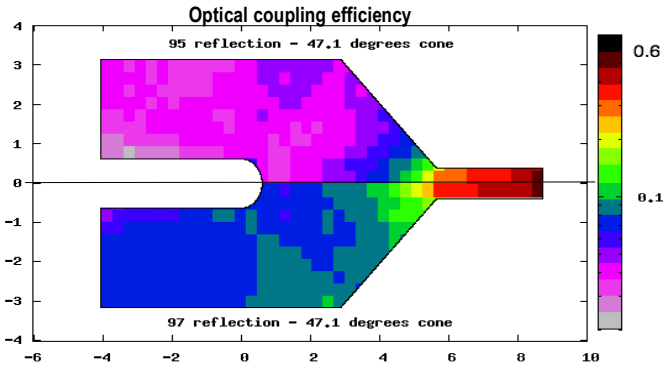

Fig. 3 Optical coupling in LCLS BLM for high-energy normally incident electrons. Upper half: reflection coefficient 0.95, lower half 0.97. The optical efficiency increases for electrons hitting near the stem and for higher reflection coefficients.

Computations ran at a speed of 100 histories/s-CPU. Each history was sorted into 3.2 x 2.0 mm^2 pixels according to its staring transverse coordinates. The resulting efficiency grids were formatted like FLUKA USRBIN detector files, so that the FLAIR[9] GNUPLOT interface could be readily used to plot the data. An example is shown in **figure 3**.

For this simple case, an analytical model based on line sources summed across image planes could also be used[8]. Both methods showed the optical efficiency to be relatively uniform over the full range of transverse locations in the radiator.

(2) Computation of the optical efficiency for realistic data

A FLUKA user routine ('mgdraw') that checks the status of a particle after it crosses an interface was edited to print, for every electron entering each BLM, the statistical weight, energy, coordinates and direction cosines. The RIBO source routine was modified to read these events from the corresponding data files. RIBO is instructed first to compute the Čerenkov angle (θ_c) as a function of the electron energy with (n_r=1.47 is the refraction index of silica, β is the relativistic ratio):

$$\cos(\theta_C) \approx \frac{1}{n_r^2 \cdot \beta} \qquad (1)$$

Then a random photon direction is sampled from the Čerenkov conical distribution in a local reference frame mounted on the impinging electron vector. The statistical weight of the photon is assigned in the source routine by multiplying the weight of the electron by Čerenkov production (N_p), given in Frank Tamm formula[10] (L is the electron path in the silica):

$$\frac{dN_p}{\partial L}\left[\frac{\gamma}{m}\right] = 2.35 \cdot 10^5 \cdot \left(1 - \frac{1}{n_r^2 \cdot \beta}\right) \qquad (2)$$

Figure 4 sketches the handshake FLUKA / RIBO.

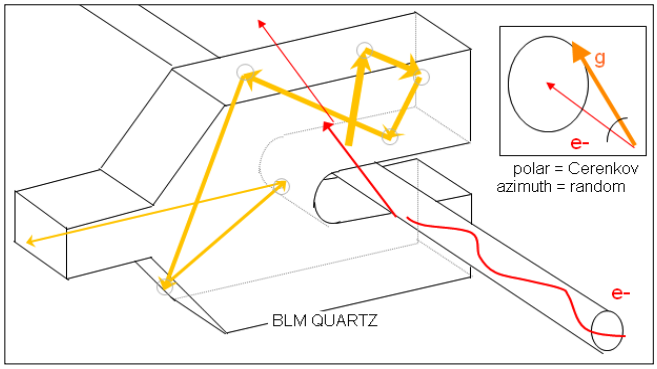

Fig. 4 Electrons that have been deviated or lost energy at insertion devices may eventually be lost and cross the BLM. There they generate Čerenkov photons that are partially absorbed throughout the multiple collisions.

II. Simulation studies

1. Study of the effect of rolling out the undulators

The LCLS undulator girders provide controls to slide the undulators off the beam pipe by up to 8 cm (towards the left). By doing so, the fragile undulator magnets are less exposed to high-energy radiation fields. **Table 1**, obtained by requesting in FLUKA a special region/reaction based scoring, shows how the relative share of photoneutron reactions in the undulator magnets is reduced by more than a factor three when the undulators are rolled out during beam finder wire bfw01 insertion at 13.6 GeV. Additionally, and for a 17 GeV e$^-$ beam, the fluence of several types of particles was scored in the upper magnets of the undulators. **Figure 5** suggests that rolling out the undulators during beam measurements can reduce the hadron fluence by an order of magnitude.

Table 1 Share [%] of photoneutron reactions along the LCLS undulator (as a function of the undulators position) for a 13.6 GeV e- beam intercepted by 40 μm beam finder wire bfw01

Undulator IN		Undulator rolled OUT	
Regions	[% (γ,n)]	Regions	[% (γ,n)]
und magnets	48.9	quadrupoles	49.5
und poles	24.7	und magnets	14.7
und pipe	15.3	und pipe	14.4
quadrupoles	5.7	other und regions	11.2
other und regions	3.2	beam pipe	10.0
beam pipe	1.9	other	0.2

2. Study of the radiation fields generated by inserting thin diagnostics

A close look at figure 5 also indicates that the maximum dose is seen by those segments located 8-10 units downbeam of the thin-target source, and that for each undulator segment the first few magnets are subject to a radiation field ten times higher than those in the back. Therefore, if an undulator needed service, it would mainly involve its first few magnets.

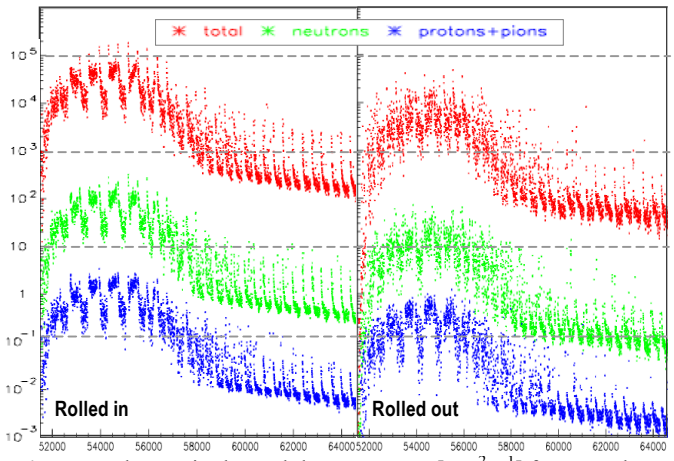

Fig. 5 Fluence in the undulator magnets [cm^{-2} s^{-1}] for every kW of 17 GeV e$^-$ beam that is intercepted by the 40 μm beam finder wire bfw01. Results are presented for rolled in / out undulators.

Photonuclear reactions and high-energy hadrons are believed[11] to be the main actors that alter the magnetic domains in $Nd_2Fe_{14}B$. Table 1 and figure 5 provide a first insight about these values at LCLS. More information can be obtained by mapping the fluence of different types/energies

of hadrons. **Figures 6** and 7 display the high-energy (> 20 MeV) hadron fluence and the nucleon and charged pion fluence along the undulator for the bfw01 source (13.6 GeV beam). Looking at the structure of these fluence maps it seems that electron[b] losses are distributed in a long portion of the undulator and that those entail showers with a non-negligible radial component. Moreover, as expected, the radiation fields are almost symmetric with respect to the horizontal beam plane, which means that the upper and lower magnets should be equally demagnetized. **Figure 8** shows the MARS15 predicted electron fluence for 1 nC beam with the same loss conditions.

Simulations have also been carried out at lower energy (9.6 GeV) and for other insertion devices, like bfw20. Comparing the fluence plot at this energy (**figure 9**) with those at 13.6 GeV we observe that the maximum fluence now takes place just 5-6 segments downstream of the insertion device.

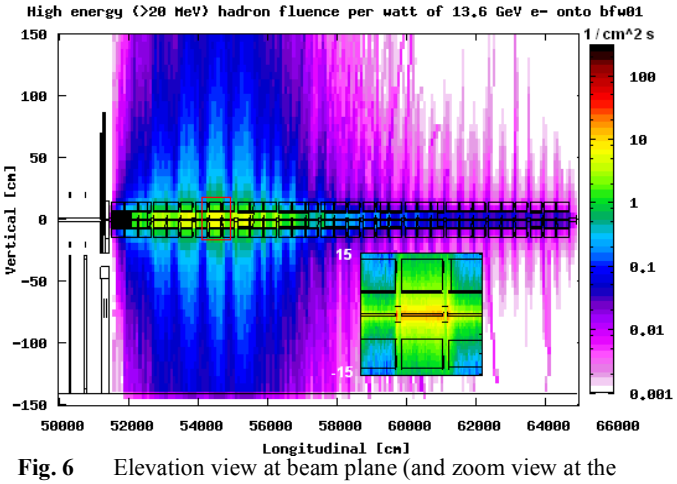

Fig. 6 Elevation view at beam plane (and zoom view at the peak) of the high-energy hadron fluence when 1 W of 13.6 GeV e^- is intercepted by bfw01

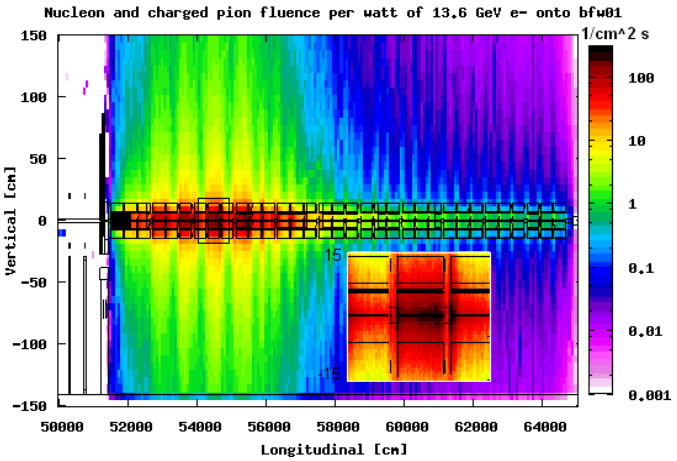

Fig. 7 Elevation view at beam plane (and zoom view at the peak) of the nucleon and $\pi^{+/-}$ fluence when 1 W of 13.6 GeV e^- is intercepted by bfw01

[b] as well as some bremsstrahlung photons generated at bfw01

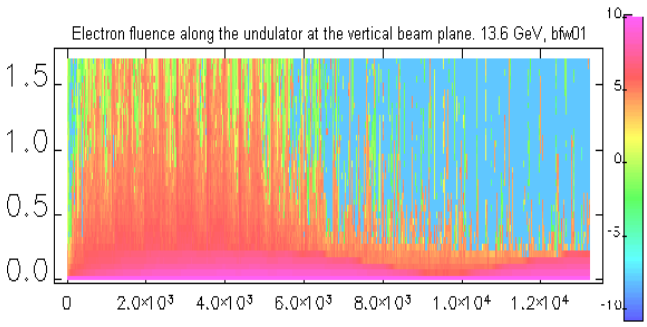

Fig. 8 Elevation view at beam plane of the electron fluence [$cm^{-2}s^{-1}$] ($\log_{10}$ scale) along the 132 m undulator when 1 nC of 13.6 GeV e^- is intercepted by bfw01. Computation performed with MARS15.

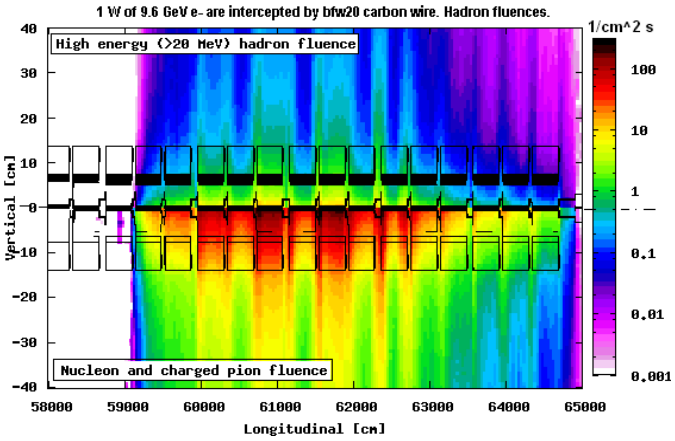

Fig. 9 Elevation view at beam plane of the hadron fluence (high-energy hadrons in top half, nucleons and $\pi^{+/-}$ in the lower half) when 1 W of 9.6 GeV e^- is intercepted by bfw20.

3. Expected signal at the PMT of the Beam Loss Monitors during beam finder wire use

The geometry of the five BLMs, including the tungsten enhancer, aluminum housing and silica reentrant fork structure was implemented in FLUKA via the prototype-lattice technique. As described in I.3.2, the 'mgdraw.f' subroutine was edited to print out the properties of all electrons entering each of the five BLMs.

Those files are used as source data for the determination of the optical coupling via the RIBO code, and they can also be individually analyzed to better understand the electron losses in the undulator. For example, the electron spectra at each BLM that appear in **figure 10** tell us that most electron energies are between 1 and 100 MeV, the average energy ranging from 15 to 20 MeV, as shown in **table 2**. Another interesting observation is that the energy distribution of electrons is very similar in each of the BLMs, which indicates that losses occur in a similar fashion along the undulator.

As advanced earlier, the electron direction shows an important radial component, with angles in the order 35-50° with respect to the **z**-axis. Individual values are listed in table 2.

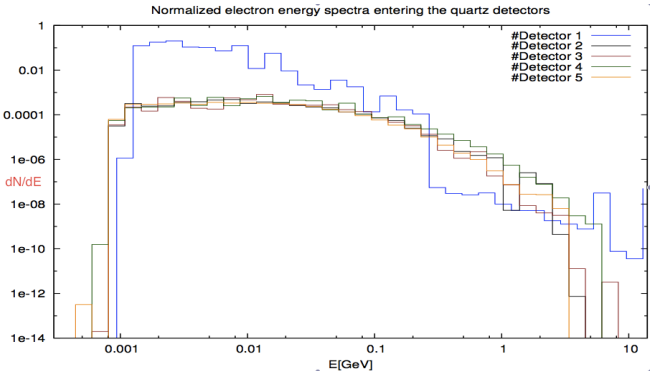

Fig. 10 Spectra of the electrons that reach each of the five installed BLMs (01, 09, 17, 25 and 33) when a 13.6 GeV e^- beam is intercepted by bfw01. Plot generated with FLAIR.

Table 2 Average properties of electrons entering the BLMs (θ_z: angle with respect to to **z**-axis, E: energy), optical coupling (η_c), electrons reaching the BLM (e^-_{BLM}) per beam electrons (e^-_B), Čerenkov photons generated in BLM (γ_{BLM}) per beam electrons, and ratio of expected peak of high-energy hadron fluence in segment 9 (F_h) versus number of photons that reach the phototubes (γ_{PC}), per 13.6 GeV e^- intercepted by bfw01

BLM	$\langle Ee^-_{BLM}\rangle$ [MeV]	$\langle\theta_z\rangle$ [°]	$\langle\eta_c\rangle$ $\cdot 10^4$	e^-_{BLM}/e^-_B	γ_{BLM}/e^-_B	$F_h/e^-_B/\gamma_{PC}$ [$cm^{-2}s^{-1}$]
01	15.7	53	7	5.6E-6	6E-4	2.1E7
09	20.4	42	176	7.6E-4	0.29	2.0E3
17	20.7	37	102	7.7E-5	0.03	3.3E4
25	24.5	34	166	2.0E-5	8E-3	7.7E4
33	19.1	41	207	1.2E-5	5E-3	1.0E5

Table 2 is the ultimate step of this study as it relates the peak high-energy hadron fluence in the undulator magnets with the expected response at the five installed beam loss monitors. It also provides information on the optical efficiency of each BLM, number of intercepted electrons and characteristics of those.

III. Conclusion and outlook

The tools to predict radiation fields and associated beam loss monitor signals have been presented. These are being refined (e.g. aperture of beam pipe sections) to better understand the meaning of the BLM readings and to improve predictions. Future upgrades and upcoming facilities (LCLS2) may benefit from these studies and computer tools.

Other operation conditions can be similarly studied by just setting up the beam conditions and/or insertion devices. For example, early simulations showed that a 465 μrad mis-steering loss triggers a sharp radiation peak short downbeam, with particle fluences about ten thousand times those shown in figure 5. Now, with BLM prediction capabilities, the signal in the BLMs could be estimated. Actually with help of Monte Carlo simulations, the pattern of signals in different BLMs could be used to determine unknown beam losses.

Separate complementary studies examine the readings of TLD dosimeters installed in different locations of the undulator tunnel.

Acknowledgment

This work was supported by Department of Energy contract DE-AC02-76SF00515

References

1) H.-D. Nuhn, "LCLS Undulator Commissioning, Alignment, and performance", 31st International Free-Electron-Laser conference (FEL09), Liverpool (UK), SLAC-PUB-13781.
2) M. Santana Leitner, "A Monte Carlo code to optimize the production of radioactive ion beams by the ISOL Technique", Ph.D. Thesis, UPC-ETSEIB (2005), CERN-THESIS-2006-031, 311 p.
3) A. Fassò, A. Ferrari, J. Ranft, and P.R. Sala, FLUKA: a multi-particle transport code, CERN-2005-10 (2005), INFN/TC_05/11, SLAC-R-773.
4) G. Battistoni, S. Muraro, P.R. Sala, F. Cerutti, A. Ferrari, S. Roesler, A. Fassò, J. Ranft, "The FLUKA code: Description and benchmarking", *Proceedings of the Hadronic Shower Simulation Workshop 2006*, Fermilab 6-8 September 2006, M. Albrow, R. Raja eds., *AIP Conference Proceeding 896,* 31-49 (2007).
5) M. Santana, J.M. Bauer, A. Fassò, J.C. Liu, X.C. Mao, A. Prinz, S.H. Rokni, T. Sanami and J. Vollaire, "Commissioning of the Electron Line of the Linac Coherent Light Source, Dose Rate Measurements and Simulations", In IAEA proceedings series STI/PUB/1433, International Topical Meeting on Nucl. Research App. And Utilization of Accel. 2009, Vienna 2009, ISBN 978-92-0-150410-4
6) N. V. Mokhov and S. I. Striganov, "Mars15 overview," Technical Report Fermilab-Conf-07/008-AD, 2007.
7) POV-ray Persistence of Vision Ray Tracer, www.povray.org
8) J. C. Dooling, W. Berg, B. X. Yang, M. Santana Leitner, A. S. Fisher and H.-D. Nuhn, "Modeling the Optical Coupling Efficiency of the Linac Coherent Light Source Beam Loss Monitor Radiator", BIW 2010 preprint, JACOW.
9) V. Vlachoudis, "FLAIR: A Powerful But User Friendly Graphical Interface For FLUKA", Proc. Int. Conf. on Mathematics, Computational Methods & Reactor Physics, (M and C 2009), Saratoga Springs, New York, 2009.
10) I. E. Tamm and I. M. Frank, Dokl. Akad. Nauk USSR 14 (1937) 109.
11) Y. Asano, T. Bizen, and X. Maréchal, *J. Synchrotron Rad*, **16** (2009), 317-324.